Effect of nitrogen content on structural and mechanical properties of AlTiZrTaHf(-N) high entropy films deposited by reactive magnetron sputtering

Mohamed El Garah, Djallel Eddine Touaibia, Sofiane Achache, Alexandre Michau, Elizaveta Sviridova, Pavel Postnikov, Mohamed Chehimi, Frederic Schuster, Frédéric Sanchette

Effect of nitrogen content on structural and mechanical properties of AlTiZrTaHf(-N) high entropy films deposited by reactive magnetron sputtering.

Mohamed El Garah,[a,b,*] Djallel Eddine Touaibia,[a,b] Sofiane Achache,[a,b] Alexandre Michau,[c] Elizaveta Sviridova, Pavel S. Postnikov,[d] Mohamed M. Chehimi,[e] Frederic Schuster,[c] Frederic Sanchette,[a,b]

[a] *LASMIS, Antenne de Nogent – 52, Pôle Technologique de Sud – Champagne, 52800 Nogent, France.*

[b] *Nogent International Center for CVD Innovation (NICCI), LRC CEA-LASMIS, Pôle Technologique de Sud – Champagne, 52800 Nogent, France*

[c] *Commissariat à l'Energie Atomique et aux énergies alternatives (CEA) Saclay, 91191 Gif-sur Yvette, France*

[d] *Research School of Chemistry and Applied Biomedical Sciences, Tomsk Polytechnic University, 634050 Tomsk, Russia*

[e] *Université de Paris, ITODYS, UMR CNRS 7086, 15 rue JA de Baïf, 75013 Paris, France*

Email : mohamed.el_garah@utt.fr

Abstract

There is a growing interest in the design of high entropy alloys due to their remarkable properties and applications in various fields such as aerospace, medical and automotive. AlTiTaZrHf(-N) high entropy metal-sublattice nitrides were deposited in various argon-nitrogen gas mixtures on glass and silicon substrates. X-ray diffraction analyses reveal a transition from amorphous to an FCC single phase by increasing the nitrogen content. The films have compact or columnar morphology depending on the nitrogen flow rate. Energy dispersive spectroscopy analysis shows a decreasing of the matals content as the nitrogen flow rates ratio $R_{N2}=N_2/Ar+N_2$ increases. XPS surface analysis reveal the formation of nitrides when the nitrogen is introduced. Evolution of hardness and Young's modulus are discussed and the maximum values are obtained for a flow rates ratio R_{N2} of 10% at 27.67 GPa and 205.56 GPa respectively. The same film reveals good tribological properties compared to other films. This work conclusively demonstrates that high entropy metal-sublattice nitrides can be generated in an efficient way with tunable properties.

Keywords: Thin films, high entropy nitrides, magnetron sputtering, surface analysis

1. Introduction

High entropy alloys (HEAs) break the design of the conventional alloys which are based on one principal element. HEAs are defined as quasi- or equimolar alloys consisting, at least, of five elementary components with an atomic percentage varying from 5 to 35 at. % [1, 2] . They become a great research hotspot in the field of metallic materials. The reported HEAs often reveal a single-phased solid solution, free of intermetallic phases. In the literature, these particular alloys are coined Multi-element Alloys MEA, Complex Component Alloys CCA, or Multielement High Entropy MHE. The ability of HEAs in forming simple solid solution phases (BCC, FCC, HCP or a mixture) make them stable and therefore reduces considerably the free-energy [3, 4]. Various investigations have been achieved to explore their physico-chemical properties revealing potential features in use of some applications [5, 6]. They exhibit excellent mechanical and physical properties such as wear resistance [7], corrosion resistance [8] and thermal stability [9]. This is why HEA are potential candidates in different critical sectors: aerospace, turbine or nuclear industries [3, 4].

Since they have been considered as promising material compared to traditional alloys, they have been investigated for high temperature applications. Like bulk HEAs, thin films of five elements or more are developed and exhibit high performance physico-chemical properties. The choice of the constituting elements is of considerable interest to control their properties. Oxidation resistance can be improved by incorporation of different elements such as Al, Cr, Ta and Si. Adding Al to other systems, *e.g.* FeCrCoNi [10], leads to transition from FCC to BCC with modification of mechanical properties. HEA containing aluminum are reported to have an enhanced oxidation resistance. Butler et al. point out that the increase of Al content enhances the oxidation resistance of AlFeCoCrNi alloy [11]. Shen et al. have deposited $(Al_{0.34}Cr_{0.22}Nb_{0.11}Si_{0.11}Ti_{0.22})_{50}N_{50}$, by using magnetron sputtering technique, pointing out also the role of Al element on the oxidation resistance of the film. Superior oxidation resistance is attributed to the formation of a dense Al_2O_3 to layer on the film surface [12].

High entropy metal-sublattice nitrides [13, 14] have been extensively studied during the last years because these alloys combine good mechanical behaviors with high thermal stabilities. These films can be deposited in reactive mode in order to control the nitrogen content. Nitrogen content has obviously significant influence on both structure and mechanical properties. Recent investigations showed the nitrogen effect on the self-organization of metallic atoms leading to phase transition [15-18]. Nitrides films are chemically inert and harder than the corresponding metallic alloys. Some films, prepared with strong nitride

forming elements (for example Al, Ti, Hf, etc.), have hardness ranging from 10 to 40 GPa [19-21], much higher than those of films containing non-nitride forming element (Co, Cu, Fe, Ni, etc.). Moreover, the nitrides films can have not only enhanced mechanical properties but also good corrosion resistance [22].

The most used techniques to deposit the nitride films are laser cladding, magnetron sputtering, spraying and electrodeposition [23]. Magnetron sputtering allows to deposit nitride films with tuned physical and chemical properties. Bombardment energy of impinging particles can be adjusted via, for instance, the bias voltage or the working pressure, which have a great effect on morphology as well as on structure and microstructure. Besides, the technique, versatile, offers the possibility to change the reactive gas (N_2, O_2, CH_4, C_2H_2).

Previous research on high-entropy nitride coatings mainly focused on their properties such as microstructure, mechanical, tribological performance and corrosion resistance are reported. The present study is focusing on the investigation of a new AlTiTaZrHf material in different Ar+N_2 atmospheres. Microstructure, chemical and mechanical properties of the high entropy metal-sublattice are discussed. The material is based on AlTiTaZrHf system, consisting of forming-nitride metal elements. Results on nitride thin films based on the Al-Ti-Ta-Zr medium entropy films have been published [18]. The addition of Hf metal is intended to promote also the formation of HfN with FCC structure [24]. Besides, HfN has been reported to influence significantly the hardness and the oxidation resistance of films [25]. Even various high entropy nitrides have already been reported in the literature, it is difficult to provide a general design rule. Investigating new high entropy nitrides become essential in the current phase of high entropy development. This work discusses how the nitriding effect influence the mechanical and tribological performance of high entropy alloy composed of strong-nitride forming elements.

2. Experimental details

2.1 Deposition

The films are deposited on glass substrates and silicon wafers by using DC magnetron sputtering of 99.99% pure high entropy equiatomic AlTiTaZrHf alloy target. The reactor is a Deph4 (DEPHIS, Etupes, France) system equipped with 4 circular cathodes 200 mm in diameter. Substrates are cleaned by subsequent ultra-sonication in acetone and ethanol (20 minutes each) followed by drying process with warm air. Afterward, the substrates are ion etched in argon (0.5 Pa) using RF power of 300 watts for a duration of 10 minutes.

The process starts with a target cleaning in argon (0.5 Pa) for a duration of 10 minutes before deposition. The discharge current on AlTiTaZrHf alloy target is kept at 2A. The target-substrate distance is kept at a distance of 10 cm. The flow rates ratio $R_{N2}=N_2/Ar+N_2$ is varied from 0 to 50%. Total pressure is maintained at 0.5 Pa. No bias or substrate heating is applied during deposition.

2.2 X-Ray Diffraction

All films were analyzed by X-ray diffraction using D8-Advance Bruker diffractometer with Cu radiation (λ=1.54 Å), θ-2θ (20-90°), step size=0.02° and step times of 1s. X-ray source is operated at 40 kV. Ni filter is used to absorb Kβ signal from monochromatic beam.

2.3 X-ray Photoelectron Spectroscopy

X-ray photoelectron spectroscopy (XPS) measurements were performed using a NEXSA apparatus (Thermo, East Grinsted, UK) fitted with a monochromatic Al Kα source (hν = 1486.6 eV). The instrument is based at TPU, Tomsk, Russian Federation. All measurements were conducted at a pressure of 10^{-9} mbar. The survey and narrow scans were recorded in the following conditions: pass energy/step size = 200/1 eV, and 40/0.1 eV, respectively. The materials are conductive and no spectral calibration was needed. In these conditions, the adventitious hydrocarbon contamination exhibited a C1s peak centered at 284.8 eV, whereas for individual nitrides the adventitious hydrocarbon contamination C1s peak slightly shift from one nitride to another [26]. We have processed the data as acquired without any charge calibration. As a matter of fact, SEM images were recorded without any metallization to compensate for static charging. Note that the samples were analyzed by XPS in Tomsk Polytechnic University implying that they have been exposed to ambient air therefore inducing some extent of unavoidable oxidation, discussed in Section 3.4. For the peak-fitting procedure, the constraints were as follows: Shirley baseline, ± 0.1 eV for binding energy position, ± 0.1 eV for FWHM, and the Laurentian to Gaussian (L/G) peak shape ratio was adjusted to get the best fit. For doublets (Hf4f, Ta4f, Zr3d and Ti2p), we have considered the binding energy splitting as well as the theoretical peak area ratios expected for f, d, and p orbitals (4/3 for $4f_{7/2}/4f_{5/2}$; 3/2 for $3d_{5/2}/3d_{3/2}$; 2/1 for $2p_{3/2}/2p_{1/2}$) as indicated in Section 3.4.

2.4 Scanning Electron Microscopy

The cross-sectional morphology of films was caried out using Hitachi SU 8030 SEM (Scanning Electron Microscope) FEG (Field Emission Gun). Their chemical composition is assessed by using SEM Hirow SH-4000M equipped with an energy dispersive x-ray

spectrometer (EDS). The measurements were carried out using voltage varying from 10 to 25KV with a working distance of 8 mm.

2.5 Nano indentation

Hardness and Young's modulus are measured by using the Nano Indenter XP, MTS Systems equipped with a three-sided pyramidal diamond tip (Berkovitch indenter). The maximum penetration depth is limited to less than 10% of the film thickness, to avoid the influence of the substrate stiffness. Hundred indents were performed for each sample and an average was calculated.

2.6 Tribological analysis

The tribological properties of the deposited high entropy metal-sublattice nitrides were investigated at room temperature by using a tribometer (CSM Instruments, High-Temperature Tribometer) under a ball-on-disk configuration. The applied normal load and sliding speed were 2 N and 0.1 m/s, respectively with a frequency of 4 Hz. The sliding distance was 96 m and the counter face was 6 mm Al_2O_3 balls.

3. Results and discussion

3.1. Deposition rate

Figure 1 shows the deposition rate as a function of R_{N2}. At $R_N = 0\%$ it is shown that the film sputtering deposition rate is 12.43 ± 0.2 nm/min. When nitrogen content in the gas mixture is increased until $R_N = 30\%$, the deposition rate of AlTiZrTaHf(-N) film drastically decreases and reaches 3.65 ± 0. 2 nm/min when R_{N2} is 30%. The main reason of this decrease is obviously target's poisoning when the nitrogen flow increases [19, 27]. Above 30% of the flow rates ratio R_N, The deposition rate is quite constant, which means that the target's surface is entirely poisoned by a nitride layer, which has a lower sputtering yield; a factor 3 compared to the metallic sputtering yield. The target's poisoning effect seems to be the predominant.

Figure 1. Sputtering deposition rate of AlTiZrTaHf(-N) high entropy films as a function of R_{N2}.

3.2. Elemental composition

Chemical composition of AlTiTaZrHf(-N) films is evaluated using scanning electron microscope equipped with Energy Dispersive Spectroscopy (EDS). The results are shown Figure 2 where an equiatomic target was used for the disposition. Without nitrogen, the film composition shows an atomic percentage varying between 19 and 22 at.% that is estimated according to EDS analysis. The metal content in the film decreases as the nitrogen flow (R_{N2}) increases up to R_{N2} = 15%. Target poisoning occurs and the sputtering yield of nitrides are very smaller than that of metals resulting in decreasing of metal amount in the films [28]. Anyway the incorporation of nitrogen in the films comes from a complex phenomenon: the target poisoning, the combination of nitrogen and metallic species in the homogeneous phase and the adsorption of nitrogen on the surface of the growing film. It is believed that the target poisoning is the preponderant phenomenon. For that reason, the deposition rate directly depends on the nitriding conditions of the target. The figure 2 tends to show that the film is a nitride for a value of R_{N2} of about 10%.

Figure 2. Chemical composition of AlTiTaZrHf(-N) films as a function of R_{N2}.

3.3. X-ray diffraction analysis

Diffraction patterns of AlTiTaZrHf(-N) HEF, as a function of the nitrogen content in the gas mixture, are shown figure 3. The films obtained at R_{N2}=0% and exhibits an amorphous structure as illustrated by the broader peaks. When the nitrogen flow is increased to 5%, AlTiTaZrHf nitride is still amorphous or nanocrystal. It is clearly seen that this halo shifts towards the lower angles at R_{N2}=5%, which means that nitrogen addition in the film leads to increase the mean distance between atoms first neighbor. High mixing entropy associated with high cooling rates of the condensation are the main reasons of the growth of amorphous phase. The high entropy can increase the mutual solubility between the element constituting the film while the large atomic size can lead to the topological instability promoting the formation amorphous structure [29]. However, as expected (section 3.2), the increase of nitrogen flow rate leads to the growth of a single-phased crystallized material and FCC solid solution is clearly detected above R_{N2}=10%. The diffractograms of this structure show five peaks (111), (200), (220), (311) and (222) as presented in the figure 3. It is no surprise knowing that Al, Ti, Ta and Hf elements can form FCC-structured nitrides with nitrogen. The same trend has been reported in the literature for various nitrides as (TiAlCrSiV)N,

(AlCrTaTiZr)N or (AlCrMoSiTi)N [21, 27, 30, 31]. Increasing the nitrogen content promotes nitrides growth that can improve the crystallinity of the films. Many studies investigated the effect of nitrogen content in HEFs and revealed that the growth of FCC solid solution phase could be due to the formation of nitrides [21, 22, 32]. In our case, the (AlTiTaZrHf(-N) films exhibit NaCl type structure. This phenomenon can be attributed to high entropy effect that enhance the mutual solubility of different elements. As shown in diffractograms, the nitride films have an out-of plane preferential orientation. The reflection (200) appears for R_{N2} values higher than 15%. The preferential orientation can be explained by the extended structure zone model (ESZM) [33]. When the energy flow toward the substrate is low, the adatoms hit the surface with nearly negligible mobility and amorphous structure can be formed. However, as the energy flow increases, the mobility of adatoms into the surface increases and crystalline structure will be formed. Mathieu et al. reported that preferred {111} orientation occurs at low N/Ti flow and {100} orientation occurs at high N/Ti flow [33]. According to that, the control of N/Metal atomic flow could promote the preferred {111} or {100} orientation.

Figure 3. Diffractograms of AlTiTaZrHf(-N) in function of R_{N2}.

Diffraction peaks of the NaCl type structure shift towards lower angles (Figure 4a), which means that the lattice distortion increases (with higher lattice parameters of AlTiTaZrHf(-N)) as the nitrogen flow increases. This phenomenon is more pronounced for higher values of R_{N2}. Figure 4b shows a linear increase of the lattice parameter with R_{N2}, which varies between 4.43 and 4.48Å. The peak shift linked to the distortion effect could be due to the residual compressive stress formed after adding the nitrogen [34].

Figure 4. a) Zoom of diffractograms showing the shift of (111) and (200) peaks. b) Lattice parameter evolution as a function of R_{N2}.

3.4. X-ray photoelectron spectroscopy (XPS) analyses

X-ray photoelectron spectroscopy was used to probe the surface chemistry of AlTiTaZrHf(-N) films. Figure 5 displays survey spectra and high-resolution core level peaks of the individual elements of the films, obtained at R_{N2}= 0% (red) and R_{N2}= 15% (blue). The survey spectra show peaks assigned to Al2p (~74 eV), Ti2p, H4f-Ta4f, O1s and N1s. Carbon s is assigned to adventitious hydrocarbon contamination whilst O1s is due to metal oxide and contamination

of the films surface. Nitrogen is absent in the surface of the film obtained at R_{N2}= 0% while at R_{N2}= 15% a strong peak of N1s is observed (Figures 5a-b). To get a deep knowledge on the surface chemistry of these films, high resolution spectra were recorded for each individual element (Figures 5b-f). XPS measurements were performed one month after deposition. Oxides formed on the top of the film surfaces upon exposure of the sample to air. On a thermodynamic point of view, oxides can be formed on the extreme surface of the films since they have low enthalpies (ΔHf°) compared to nitrides (Table 1). For this reason, in this section, we focus only on the formation of nitrides.

Without nitrogen, Al2p spectrum (Figure 5c, red spectrum) shows the presence of metallic Al2p. At R_{N2}= 15%, a transformation of metallic Al to AlN can be clearly seen. The peak of metallic Al2p disappears and AlN is observed at 73.2. Compared to red peak, the blue one is broad, therefore showing the presence of AlN (Al_2O_3 is present because of contamination). Figure 5d shows that Ti is present at metallic state as judged from the $Ti2p_{3/2}$ peak position at 453.0 eV [35], when R_{N2}= 0%. At R_{N2}= 15%, TiN is detected at 455.1 eV [36]. The $Ti2p_{3/2}$ peak of metallic Ti disappears after increasing the nitrogen. Zr high resolution spectra (Figure 5e) show the presence of metallic $Zr3d_{5/2}$ at 177.9 eV [37], when R_{N2}= 0%. Increasing the nitrogen flow rate leads to the formation of ZrN at 180.5 eV. The value for ZrN is close to 180.9 eV, reported by Badrinarayanan *et al*. [38]. Quasi no Zr3d from metallic Zr was detected at R_{N2}= 15% (Figure 5e). Ta exhibits a Ta4f peak doublet assigned to the metallic state; *i.e.* $Ta4f_{7/2}$ centred at 21.0 eV [39], when R_{N2}= 0% (Figure 5f). At R_{N2}= 15%, metallic Ta disappears and TaN is formed and show $Ta4f_{7/2}$ peaks centered at 24.3 eV. The same tendency is observed for Hf (Figure 5f). $Hf4f_{7/2}$ peak due to metallic Hf is observed at 13.2 eV for R_{N2}= 0%. At R_{N2}= 15%, a transformation of metallic Hf to HfN is recorded. This compound is corresponding to $Hf4f_{7/2}$ peaks centred at 15.6 eV.

For the sake of clarity, we have displayed only the untreated and one HEA doped with nitrogen. For all samples, we have peak fitted all important peaks taking into account the constraints of peak separation in doublets (Hf4f, Ta4f, Zr3d and Ti2p) and the theoretical ratios (4/3 for $4f_{7/2}/4f_{5/2}$; 3/2 for $3d_{5/2}/3d_{3/2}$; 2/1 for $2p_{3/2}/2p_{1/2}$). This permitted to peak fit all spectra and determine surface chemical composition of all samples. By introducing the nitrogen during the deposition process, atomic percent of the elements decreases due to the formation of nitrides. Nitrided elements are then sputtered and deposited into the surface leading to the formation of textured films depending on the introduced nitrogen flow.

Table 1. Enthalpy of formation of oxides and nitrides of different elements constituting the films [40-42].

Figure 5. XPS spectra of AlTiTaZrHf(-N) films at R_{N2} = 0% (red, bottom spectra) and R_{N2} =15% (blue, upper spectra): survey (a), N1s (b), Al2p (c), Ti2p (d), Zr3d (e), and Hf4f-Ta4f (f).

3.5. Morphology

Fracture cross-sectional SEM images of all film, in function of the nitrogen flow rate, are presented in the figure 6. The films with metallic structure, obtained at R_{N2}= 0% and 5%, have a compact morphology, related the low deposition pressure. Indeed, the mean free path in the plasma is high at low deposition pressure. Thus, the adatoms have enough energy to fill the voids between grains, which increases the film density.

However, from R_{N2}= 10% to 50% a columnar structure emerges. The film at 10% presents columns less dense compared to that of the film at 40%. The density increases as the nitrogen flow increases. Mathieu et al. [33] calculated the energy flux incident at the growing film in the case of TiN and revealed that the mobility of the growing plane increases as the nitrogen flow rate increases. This could be the main reason for the increasing of the density of the film when R_{N2} varies from 10 to 50%.

Figure 6. Cross-sectional SEM image of AlTiTaZrHf(-N) as a function of R_{N2}.

3.6. Mechanical and tribological properties

3.6.1. Hardness and Young's modulus

The mean grain size of the nitride phase is estimated using the Scherrer equation from the most intense (111) reflection (Figure 7a). The mean grains size is ranged from 300 to 480 nm and 3 zones (R1, R2 and R3) can be distinguished. The mean grain size decreases when R_{N2} is between 10% and 15% (R1 zone) and above R_{N2}=30% (R3 zone). It increases when R_{N2} is in the range 15% to 30%.

Evolution of mechanical properties (Hardness and Young Modulus) of AlTiTaZrHf(-N) is presented in figure 7b. Hardness and Young's modulus are in the ranges 7.85 GPa to 27.67

GPa and 109.33 GPa to 205.5 GPa, respectively. The microstructure refinement and the lattice distortion seem to drive the mechanical properties when the nitrogen content in the gas mixture increases.

Figure 7. a) Mean grains size evolution as a function of R_{N2}. b) Hardness and Young's modulus of AlTiTaZrHf(-N) as a function of R_{N2}.

3.6.2. Toughness and crack resistance

In general way, the tribological properties of films can be predicted via their mechanical properties under nanoindentation. Toughness and crack resistance can be predicted from two ratios: elasticity index (H/E) and plasticity index (H^3/E^2) respectively [43]. Higher values of both H/E and H^3/E^2 ratios may indicate good tribological performance of the films. The maximum values of H/E and H^3/E^2 (0.135 and 0.5 respectively) are obtained for AlTiTaZrHf(-N) film deposited at R_{N2}=10% (Figure 8). As R_{N2} increases from 0% to 10%, both H/E and H^3/E^2 ratios increase from 0.071 to 0.135 and from 0.041 to 0.050, respectively. However, when R_{N2} increase H/E remains constant until R_{N2}=30% followed by a decreasing to 0.111 while H^3/E^2 starts to decrease and reaches 0.253 (Figure 8).

Ren et al. reported a variation of tribological properties of $(AlCrMnNiZrB_{0.1})N_x$ films as a function of nitrogen flow rate [44]. The results reveal a variation of H/E and H^3/E^2 ratios depending on the variation of N/Ar flow rate. High value of H/E and H^3/E^2 are obtained of $(AlCrMnNiZrB_{0.1})N_x$ deposited with N_2/Ar=0.5. Furthermore, the same film i.e. deposited at N_2/Ar=0.5, exhibits a low friction coefficient. This result confirms that the high values of H/E and H^3/E^2 ratios are associated with good tribological properties of nitrides films. In our case, high H/E and H^3/E^2 are obtained for film R_{N2}=10% which could present excellent property for the resistance to plastic deformation.

Figure 8. H/E and H^3/E^2 ratio of AlTiTaZrHf(-N) films in function of R_{N2}.

3.6.3. Friction coefficient

Figure 9 show the friction coefficient of AlTiTaZrHf(-N) films for different nitrogen flow. The friction coefficient of AlTiTaZrHf is measured at 0.95. By increasing the nitrogen flow the friction coefficient first decreases and then increases. At R_{N2}= 10%, the friction coefficient of AlTiTaZrHf(-N) films reaches the lowest value of 0.7. As the nitrogen flow increases from

R_{N2}=20% to 30%, the friction coefficient increases. However, when the nitrogen continuous to increase > 30% the friction coefficient decreases. This trend my due to increasing of nitrogen content in the film increases leading to the refining of the structure.

As mentioned above, XRD analysis (cf. figure 4) revealed a widening of peaks when R_{N2}>30%.

The results are in good agreement with the calculated H/E and H^3/E^2 reports revealing the high mechanical and tribological properties of the film obtained at R_{N2}=10%.

Figure 9. Fiction coefficient of AlTiTaZrHf(-N) films as a function of R_{N2}.

4. Conclusion

AlTiTaZrHf(-N) HEFs are deposited by magnetron sputtering of a target with equiatomic composition in different Ar+N_2 atmospheres. The increase of flow rates ratio (R_{N2}=N_2/Ar+N_2) in the chambre leads to a drop in the deposition rate up to R_{N2} of 30% and a decrease in metallic elements content up to R_{N2} of 15% and these values stabilize for the higher nitrogen contents in the gas mixture. Films are amorphous single-phased without nitrogen and a FCC single phased material is detected for higher R_{N2} flow rates ratios. All the as-deposited films have a non-columnar compact morphology.

Maximum values of hardness and Young's modulus are measured at 27.67 GPa and 205.56 GPa respectively and they are obtained for film deposited at R_{N2}=10%. The increase of hardness and Young's modulus is mainly explained by nitride growth and evolution of the mean grain size. The film obtained at R_{N2}=10% exhibits the highest H/E and H^3/E^2 ratios and good tribological performances are then expected. This film has the lowest friction coefficient against aluminum oxide ball (Φ 6 mm) due to the compact film.

XPS analysis revealed the formation of nitrides of all elements constituting the films. Oxides are formed on the surface of films due to their low enthalpy energy compared to that of nitrides.

Acknowledgements

This works was financially supported by Groupement d'Intérêt Public Haute-Marne and Commissariat à l'Energie Atomique et aux Energies Alternatives (CEA). Annual funding (no funding number).

References

[1] J. Yeh, S. Chen, S. Lin, J. Gan, T. Chin, T. Shun, C. Tsau, S. Chang, Nanostructured high-entropy alloys with multiple principal elements: novel alloy design concepts and outcomes, Adv. Eng. Mater., 6 (2004) 299-303.
[2] B. Cantor, I. Chang, P. Knight, A. Vincent, Microstructural development in equiatomic multicomponent alloys, Mater. Sci. Eng. A, 375 (2004) 213-218.
[3] J. Li, Y. Huang, X. Meng, Y. Xie, A review on high entropy alloys coatings: fabrication processes and property assessment, Adv. Eng. Mater., 21 (2019) 1900343.
[4] X.H. Yan, J.S. Li, W.R. Zhang, Y. Zhang, Physics, A brief review of high-entropy films, Mater. Chem., 210 (2018) 12-19.
[5] Y. Zhang, T.T. Zuo, Z. Tang, M.C. Gao, K.A. Dahmen, P.K. Liaw, Z.P. Lu, Microstructures and properties of high-entropy alloys, Prog. Mater. Sci., 61 (2014) 1-93.
[6] B. Gludovatz, A. Hohenwarter, D. Catoor, E.H. Chang, E.P. George, R.O. Ritchie, A fracture-resistant high-entropy alloy for cryogenic applications, Science, 345 (2014) 1153-1158.
[7] J.B. Cheng, X.B. Liang, B.S. Xu, Effect of Nb addition on the structure and mechanical behaviors of CoCrCuFeNi high-entropy alloy coatings, Surf. Coat. Technol., 240 (2014) 184-190.
[8] H.-T. Hsueh, W.-J. Shen, M.-H. Tsai, J.-W. Yeh, Effect of nitrogen content and substrate bias on mechanical and corrosion properties of high-entropy films (AlCrSiTiZr) 100− xNx, Surf. Coat. Technol., 206 (2012) 4106-4112.
[9] W. Sheng, X. Yang, C. Wang, Y. Zhang, Nano-crystallization of high-entropy amorphous NbTiAlSiWxNy films prepared by magnetron sputtering, Entropy, 18 (2016) 226.
[10] S.C. Middleburgh, D.M. King, G.R. Lumpkin, M. Cortie, L. Edwards, Segregation and migration of species in the CrCoFeNi high entropy alloy, J. Alloys Compd., 599 (2014) 179-182.
[11] T.M. Butler, M.L. Weaver, Oxidation behavior of arc melted AlCoCrFeNi multi-component high-entropy alloys, J. Alloy. Compoun., 674 (2016) 229-244.
[12] W.J. Shen, M.H. Tsai, K.Y. Tsai, C.C. Juan, C.W. Tsai, J.W. Yeh, Y.S. Chang, Superior oxidation resistance of (Al0. 34Cr0. 22Nb0. 11Si0. 11Ti0. 22) 50N50 high-entropy nitride, J. Electrochem. Soc., 160 (2013) C531-C535.
[13] J.M.J.J.o.A.P. Schneider, How high is the entropy in high entropy ceramics?, 130 (2021) 150903.
[14] A. Kirnbauer, A. Kretschmer, C.M. Koller, T. Wojcik, V. Paneta, M. Hans, J.M. Schneider, P. Polcik, P.H. Mayrhofer, Mechanical properties and thermal stability of reactively sputtered multi-principal-metal Hf-Ta-Ti-V-Zr nitrides, Surface and Coatings Technology, 389 (2020) 125674.
[15] P. Cui, W. Li, P. Liu, K. Zhang, F. Ma, X. Chen, R. Feng, P.K. Liaw, Effects of nitrogen content on microstructures and mechanical properties of (AlCrTiZrHf) N high-entropy alloy nitride films, J. Alloys Compd, 834 (2020) 155063.
[16] N.A. Khan, B. Akhavan, C. Zhou, H. Zhou, L. Chang, Y. Wang, Y. Liu, M.M. Bilek, Z. Liu, High entropy nitride (HEN) thin films of AlCoCrCu0. 5FeNi deposited by reactive magnetron sputtering, Surf. Coat. Technol., 402 (2020) 126327.
[17] C. Sha, Z. Zhou, Z. Xie, P. Munroe, FeMnNiCoCr-based high entropy alloy coatings: Effect of nitrogen additions on microstructural development, mechanical properties and tribological performance, J. Appl. Surf. Sci., 507 (2020) 145101.
[18] M. El Garah, S. Achache, A. Michau, F. Schuster, F. Sanchette, Structural and mechanical properties of AlTiTaZr (N) medium entropy films (MEF) obtained by DC magnetron sputtering in dynamic mode, Surf. Coat. Technol., 396 (2020) 125941.

[19] H.-W. Chang, P.-K. Huang, A. Davison, J.-W. Yeh, C.-H. Tsau, C.-C. Yang, Nitride films deposited from an equimolar Al–Cr–Mo–Si–Ti alloy target by reactive direct current magnetron sputtering, Thin Solid Films, 516 (2008) 6402-6408.
[20] Z.-C. Chang, S.-C. Liang, S. Han, Effect of microstructure on the nanomechanical properties of TiVCrZrAl nitride films deposited by magnetron sputtering, Nucl. Instrum. Methods Phys. Res., 269 (2011) 1973-1976.
[21] K.-H. Cheng, C.-H. Lai, S.-J. Lin, J.-W. Yeh, Structural and mechanical properties of multi-element (AlCrMoTaTiZr)Nx coatings by reactive magnetron sputtering, Thin Solid Films, 519 (2011) 3185-3190.
[22] R. Chen, Z. Cai, J. Pu, Z. Lu, S. Chen, S. Zheng, C. Zeng, Effects of nitriding on the microstructure and properties of VAlTiCrMo high-entropy alloy coatings by sputtering technique, J. Alloys Compd, 827 (2020) 153836.
[23] W. Li, P. Liu, P.K. Liaw, Microstructures and properties of high-entropy alloy films and coatings: a review, Mater. Res. Lett., 6 (2018) 199-229.
[24] M.A. Bab, L. Mendoza-Zélis, L.C. Damonte, Nanocrystalline HfN produced by mechanical milling: Kinetic aspects, Acta Materialia, 49 (2001) 4205-4213.
[25] D.A.R. Fernandez, B.S.S. Brito, I.A.D. Santos, V.F.D. Soares, A.R. Terto, G.B. de Oliveira, R. Hubler, W.W. Batista, E.K. Tentardini, Effect of hafnium contaminant present in zirconium targets on sputter deposited ZrN thin films, Nucl. Instrum. Methods Phys. Res., B, 462 (2020) 90-94.
[26] G. Greczynski, L.J.C. Hultman, C 1s peak of adventitious carbon aligns to the vacuum level: dire consequences for material's bonding assignment by photoelectron spectroscopy, 18 (2017) 1507.
[27] C.-H. Lai, S.-J. Lin, J.-W. Yeh, S.-Y. Chang, Preparation and characterization of AlCrTaTiZr multi-element nitride coatings, Surf. Coat. Technol., 201 (2006) 3275-3280.
[28] L. Chen, W. Li, P. Liu, K. Zhang, F. Ma, X. Chen, H. Zhou, X.J.V. Liu, Microstructure and mechanical properties of (AlCrTiZrV) Nx high-entropy alloy nitride films by reactive magnetron sputtering, 181 (2020) 109706.
[29] D.-C. Tsai, Y.-L. Huang, S.-R. Lin, S.-C. Liang, F.-S. Shieu, Effect of nitrogen flow ratios on the structure and mechanical properties of (TiVCrZrY)N coatings prepared by reactive magnetron sputtering, Applied Surface Science, 257 (2010) 1361-1367.
[30] B. Ren, S. Yan, R. Zhao, Z. Liu, Structure and properties of (AlCrMoNiTi) Nx and (AlCrMoZrTi) Nx films by reactive RF sputtering, Surf. Coat. Technol., 235 (2013) 764-772.
[31] C. Lin, J. Duh, J. Yeh, Multi-component nitride coatings derived from Ti–Al–Cr–Si–V target in RF magnetron sputter, Surf. Coat. Technol., 201 (2007) 6304-6308.
[32] B. Ren, Z. Shen, Z. Liu, Structure and mechanical properties of multi-element (AlCrMnMoNiZr)Nx coatings by reactive magnetron sputtering, J. Alloy. Compoun., 560 (2013) 171-176.
[33] S. Mahieu, P. Ghekiere, D. Depla, R. De Gryse, Biaxial alignment in sputter deposited thin films, Thin Solid Films, 515 (2006) 1229-1249.
[34] H. Li, N. Jiang, J. Li, J. Huang, J. Kong, D. Xiong, Hard and tough (NbTaMoW)Nx high entropy nitride films with sub-stoichiometric nitrogen, Journal of Alloys and Compounds, 889 (2021) 161713.
[35] D. Simon, C. Perrin, J. Bardolle, ESCA study of Nb and Ti oxides. Applications to the determination of the nature of the superficial films formed during the oxidation of Nb-Ti and Nb-Ti alloys, J. Microsc. Spectrosc. Electron., 1 (1976).
[36] A. Bagdasaryan, A. Pshyk, L. Coy, P. Konarski, M. Misnik, V. Ivashchenko, M. Kempiński, N. Mediukh, A. Pogrebnjak, V. Beresnev, A new type of (TiZrNbTaHf) N/MoN nanocomposite coating: Microstructure and properties depending on energy of incident ions, Compos. Part B: Eng. , 146 (2018) 132-144.

[37] I. Takano, S. Isobe, T. Sasaki, Y. Baba, Nitrogenation of various transition metals by N+ 2-ion implantation, Appl. Surf. Sci., 37 (1989) 25-32.
[38] S. Badrinarayanan, S. Sinha, A.B. Mandale, XPS studies of nitrogen ion implanted zirconium and titanium, Journal of Electron Spectroscopy and Related Phenomena, 49 (1989) 303-309.
[39] S. Badrinarayanan, S. Sinha, X-ray photoelectron spectroscopy studies of the reaction of N+ 2-ion beams with niobium and tantalum metals, J. Appl. Phys., 69 (1991) 1141-1146.
[40] S. Elder, F. DiSalvo, L. Topor, A. Navrotsky, Thermodynamics of ternary nitride formation by ammonolysis: application to lithium molybdenum nitride (LiMoN2), sodium tungsten nitride (Na3WN3), and sodium tungsten oxide nitride (Na3WO3N), J. Chem. Matter., 5 (1993) 1545-1553.
[41] S.V. Ushakov, A. Navrotsky, Q.-J. Hong, A. van de Walle, Carbides and nitrides of zirconium and hafnium, Materials, 12 (2019) 2728.
[42] A. Kornilov, I. Ushakova, E. Huber Jr, C. Holley Jr, The enthalpy of formation of hafnium dioxide, J. Chem. Thermodyn., 7 (1975) 21-26.
[43] A. Leyland, A. Matthews, On the significance of the H/E ratio in wear control: a nanocomposite coating approach to optimised tribological behaviour, Wear, 246 (2000) 1-11.
[44] B. Ren, Z.X. Liu, L. Shi, B. Cai, M.X. Wang, Structure and properties of (AlCrMnMoNiZrB0.1)Nx coatings prepared by reactive DC sputtering, Appl. Surf. Sci., 257 (2011) 7172-7178.

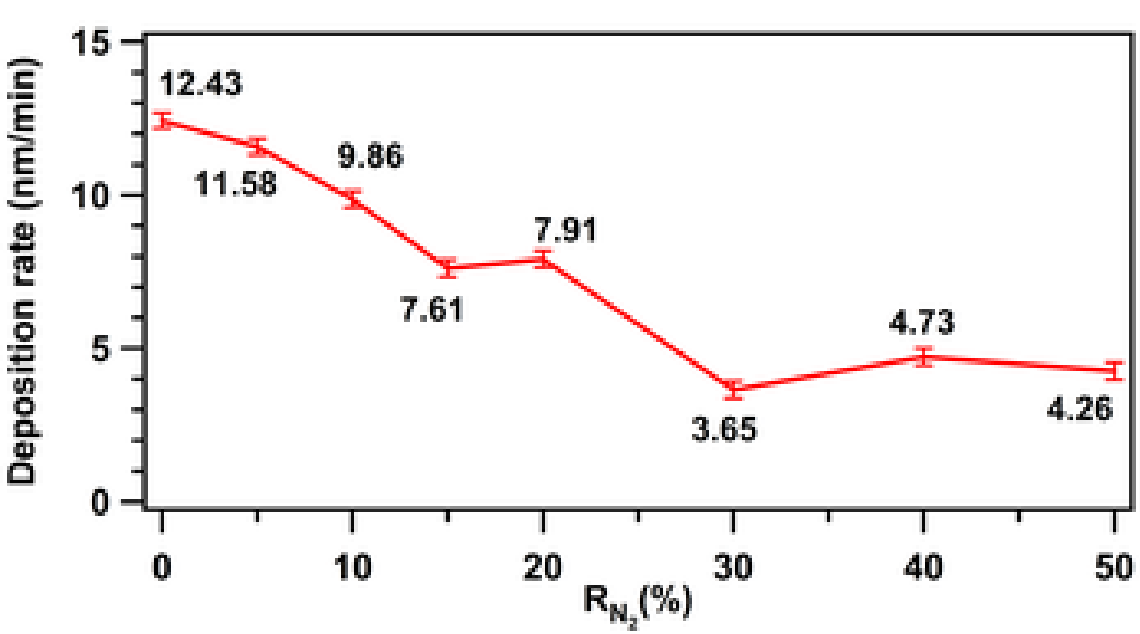
Deposition rate (nm/min)
15
10
5
0
12.43
11.58
9.86
7.61
7.91
3.65
4.73
4.26
0
10
20
30
40
50
R_{N_2}(%)

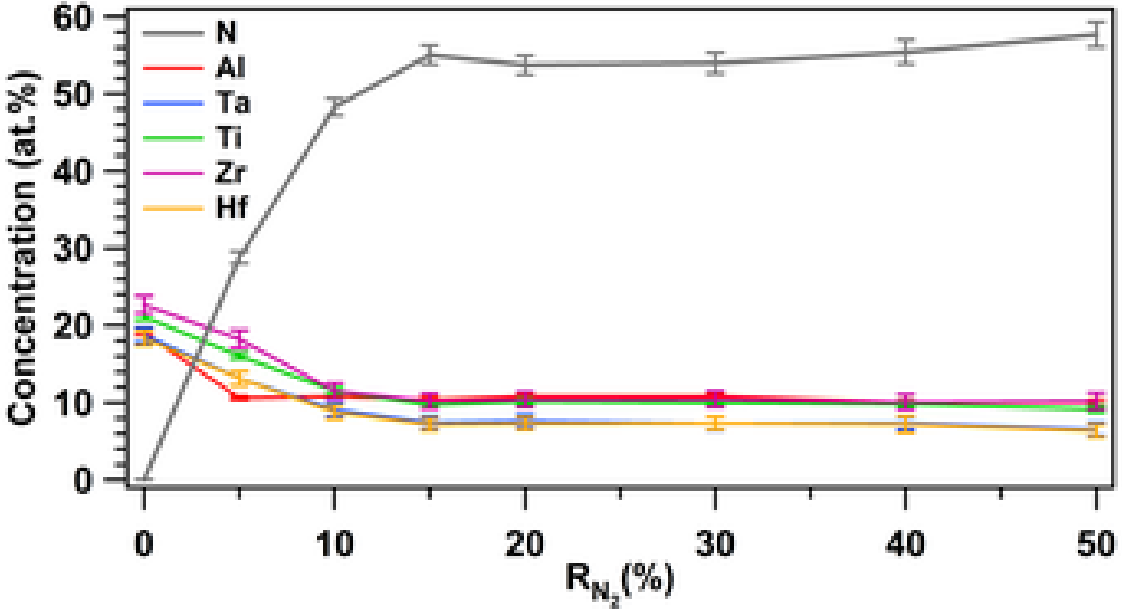
N
Al
Ta
Ti
Zr
Hf
Concentration (at.%)
0
10
20
30
40
50
60
0
10
20
30
40
50
R_{N_2}(%)

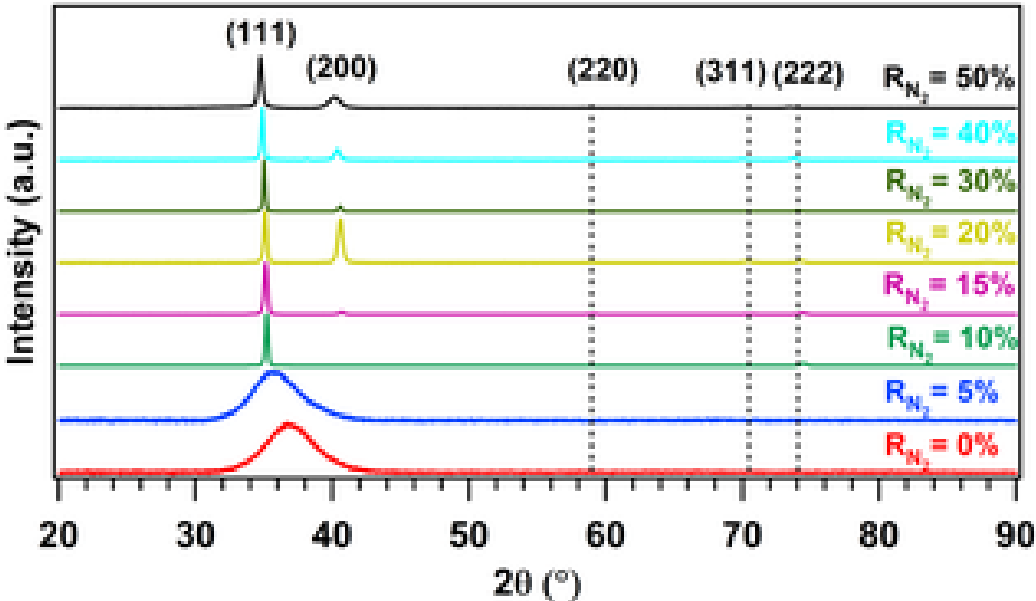
(111)
(200)
(220)
(311) (222)
R_{N_2} = 50%
R_{N_2} = 40%
R_{N_2} = 30%
R_{N_2} = 20%
R_{N_2} = 15%
R_{N_2} = 10%
R_{N_2} = 5%
R_{N_2} = 0%
Intensity (a.u.)
20
30
40
50
60
70
80
90
2θ (°)

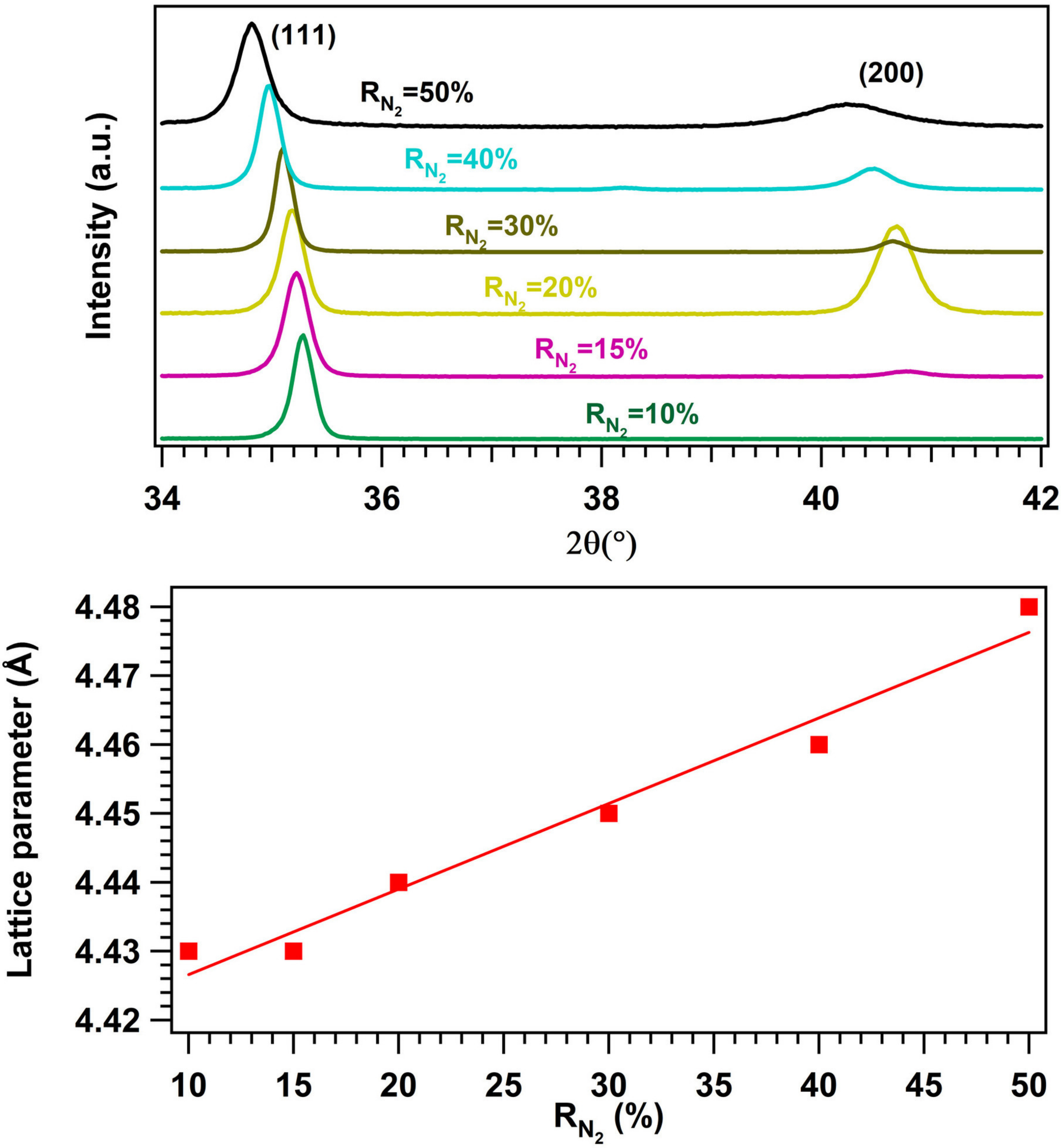
(111)
(200)
R_{N_2}=50%
R_{N_2}=40%
R_{N_2}=30%
R_{N_2}=20%
R_{N_2}=15%
R_{N_2}=10%
Intensity (a.u.)
34
36
38
40
42
2θ(°)
Lattice parameter (Å)
4.48
4.47
4.46
4.45
4.44
4.43
4.42
10
15
20
25
30
35
40
45
50
R_{N_2} (%)

a)

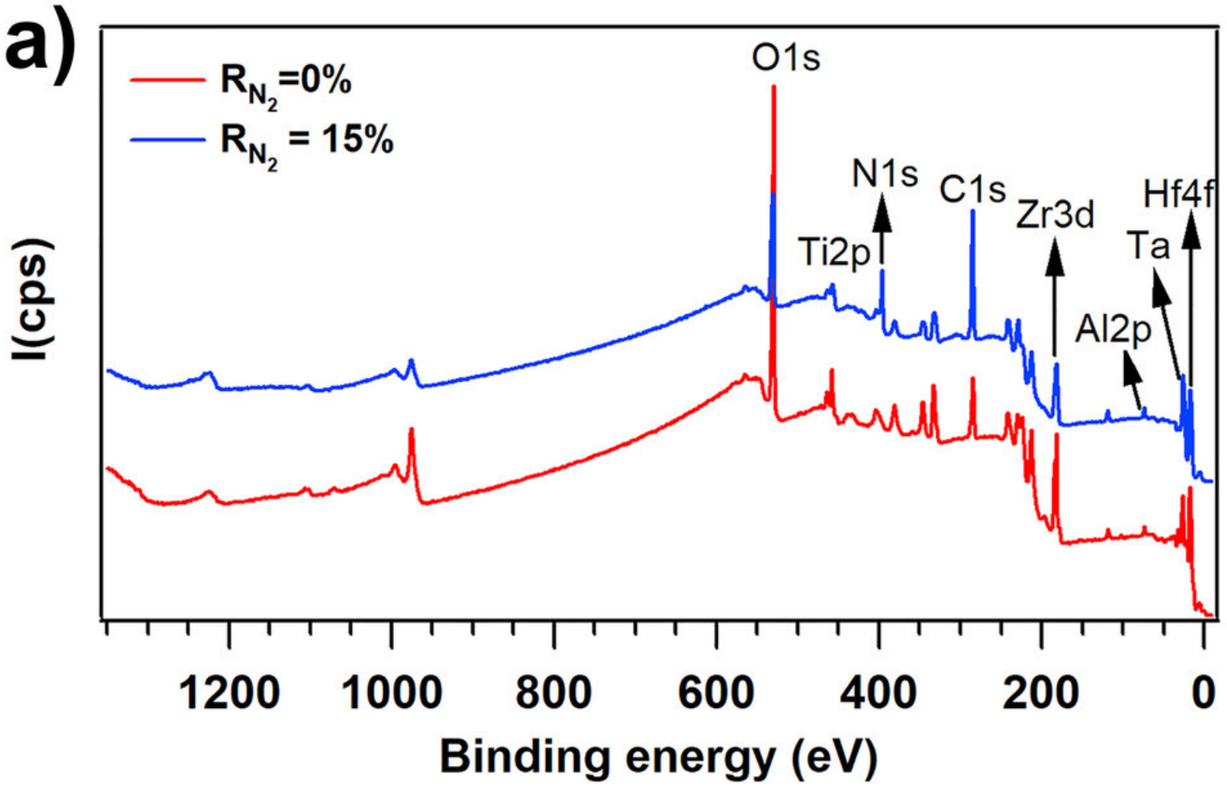
R_{N_2}=0%
R_{N_2} = 15%
O1s
N1s
C1s
Zr3d
Hf4f
Ti2p
Ta
Al2p
I(cps)
1200
1000
800
600
400
200
0
Binding energy (eV)

b)

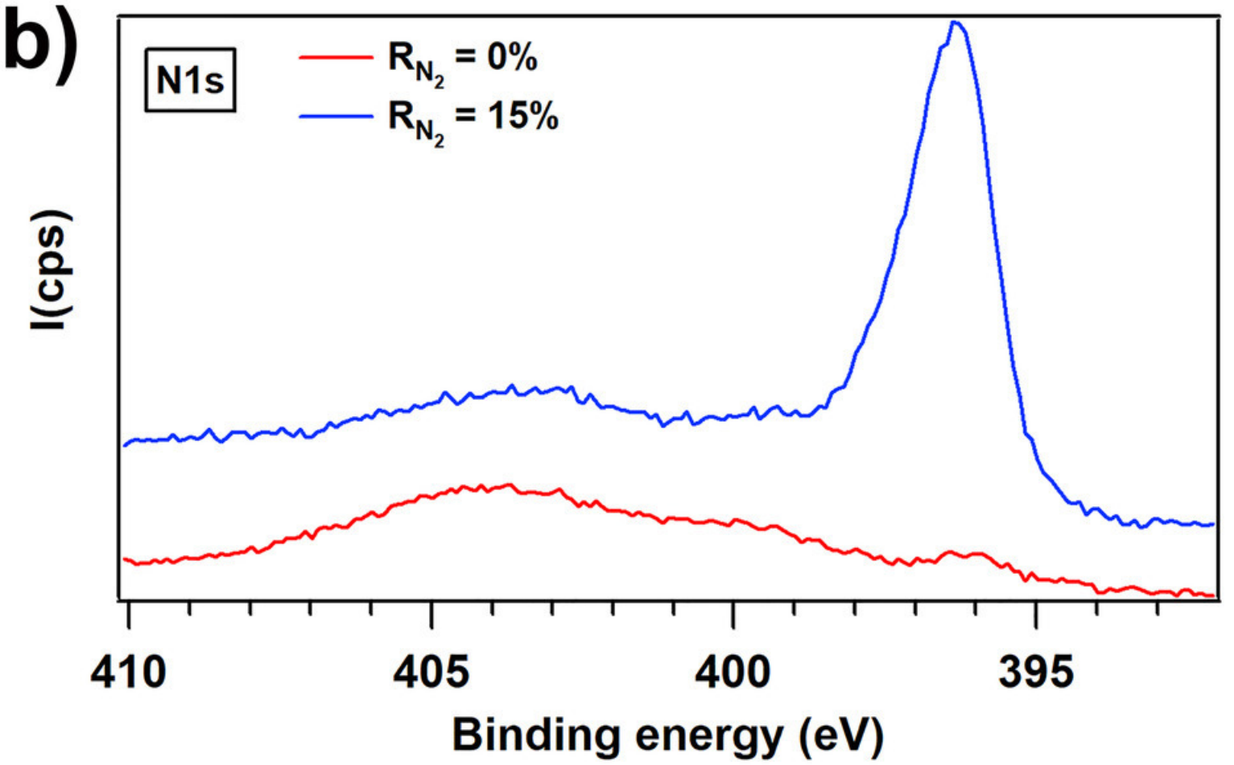
N1s
R_{N_2} = 0%
R_{N_2} = 15%
I(cps)
410
405
400
395
Binding energy (eV)

c)

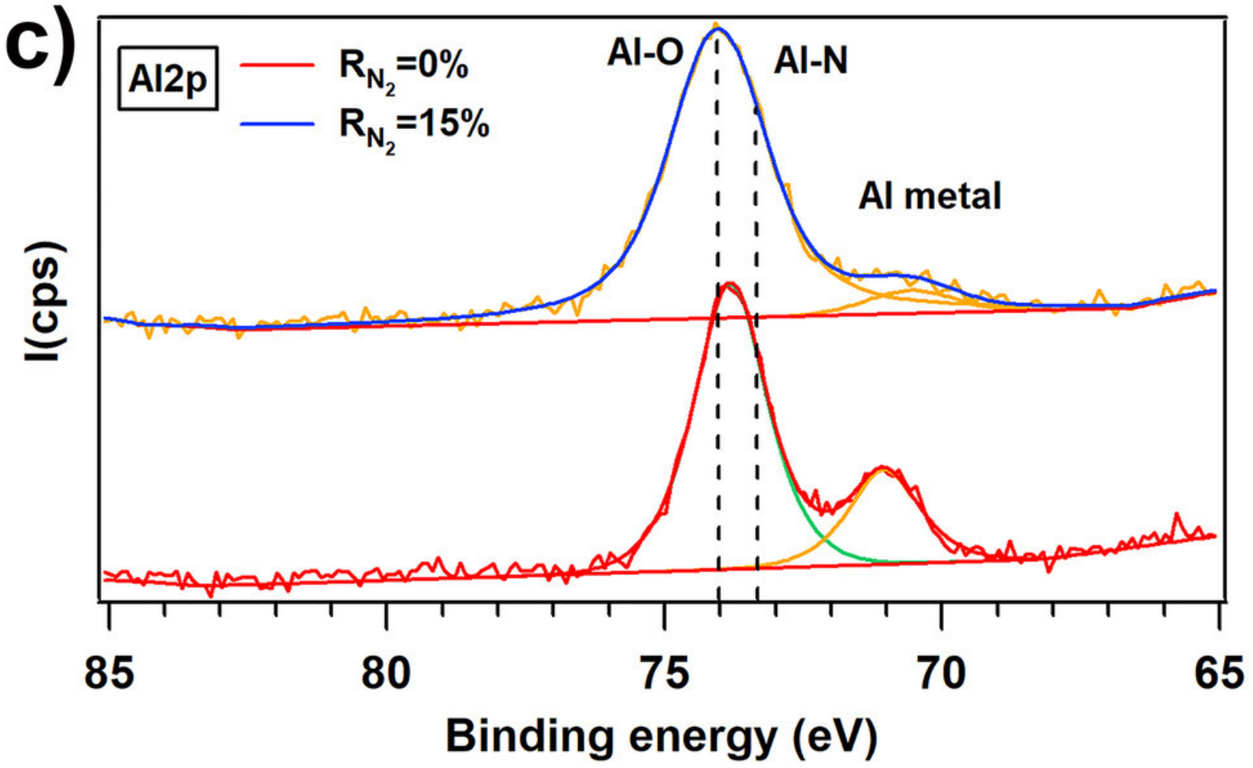
Al2p
R_{N_2}=0%
R_{N_2}=15%
Al-O
Al-N
Al metal
I(cps)
85
80
75
70
65
Binding energy (eV)

d)

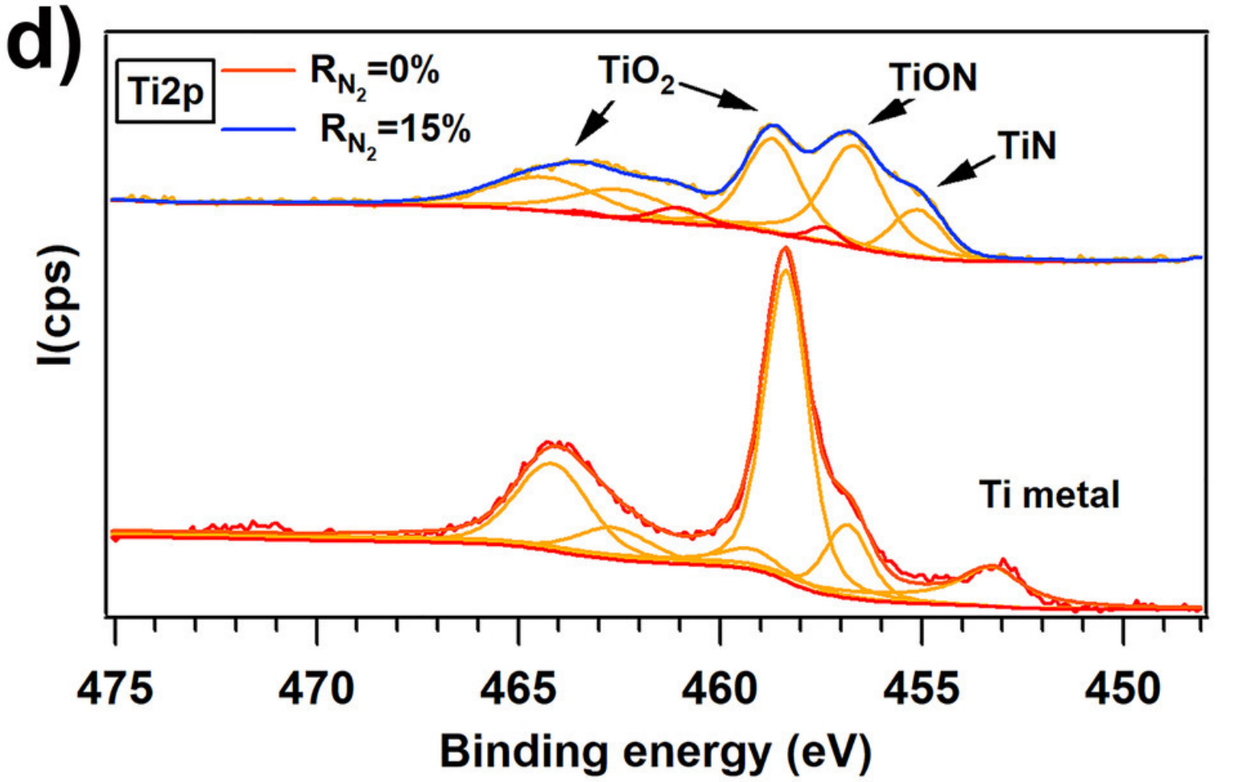
Ti2p
R_{N_2}=0%
R_{N_2}=15%
TiO_2
TiON
TiN
Ti metal
I(cps)
475
470
465
460
455
450
Binding energy (eV)

e)

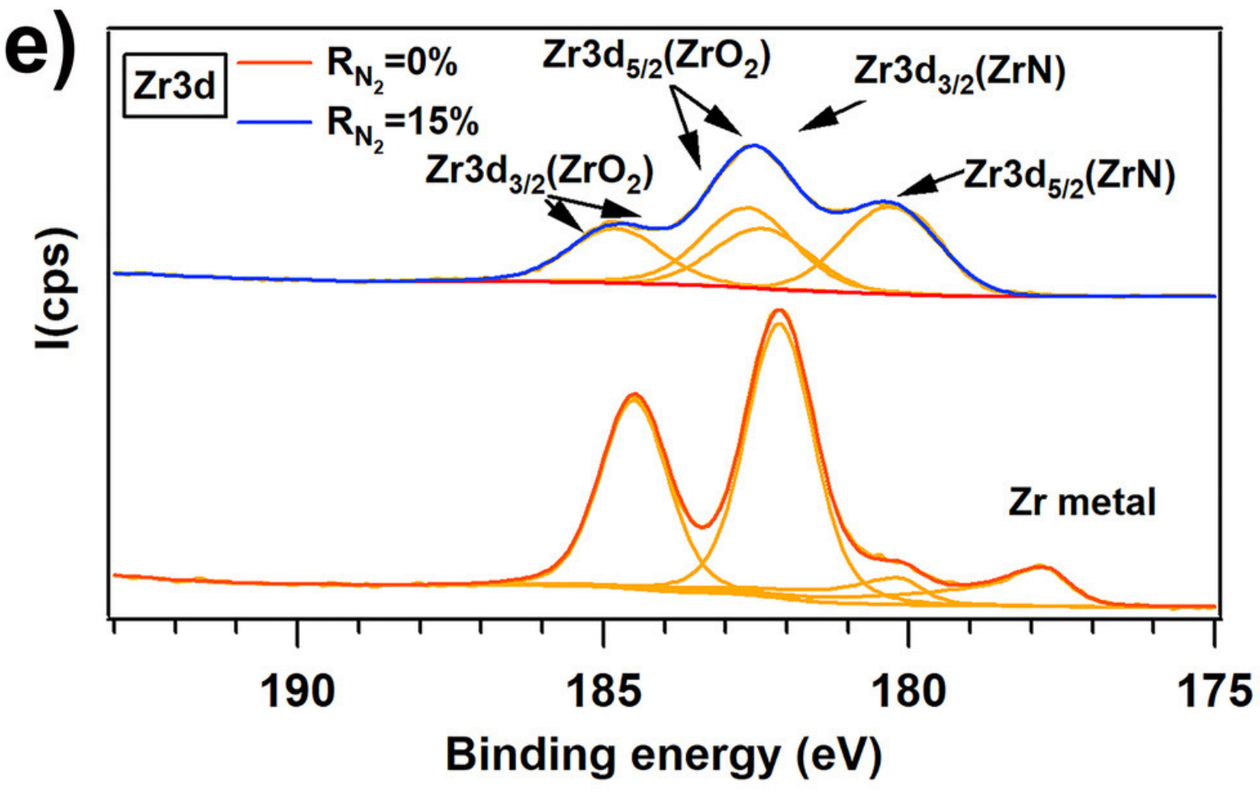
Zr3d
R_{N_2}=0%
R_{N_2}=15%
$Zr3d_{5/2}(ZrO_2)$
$Zr3d_{3/2}(ZrN)$
$Zr3d_{3/2}(ZrO_2)$
$Zr3d_{5/2}(ZrN)$
Zr metal
I(cps)
190
185
180
175
Binding energy (eV)

f)

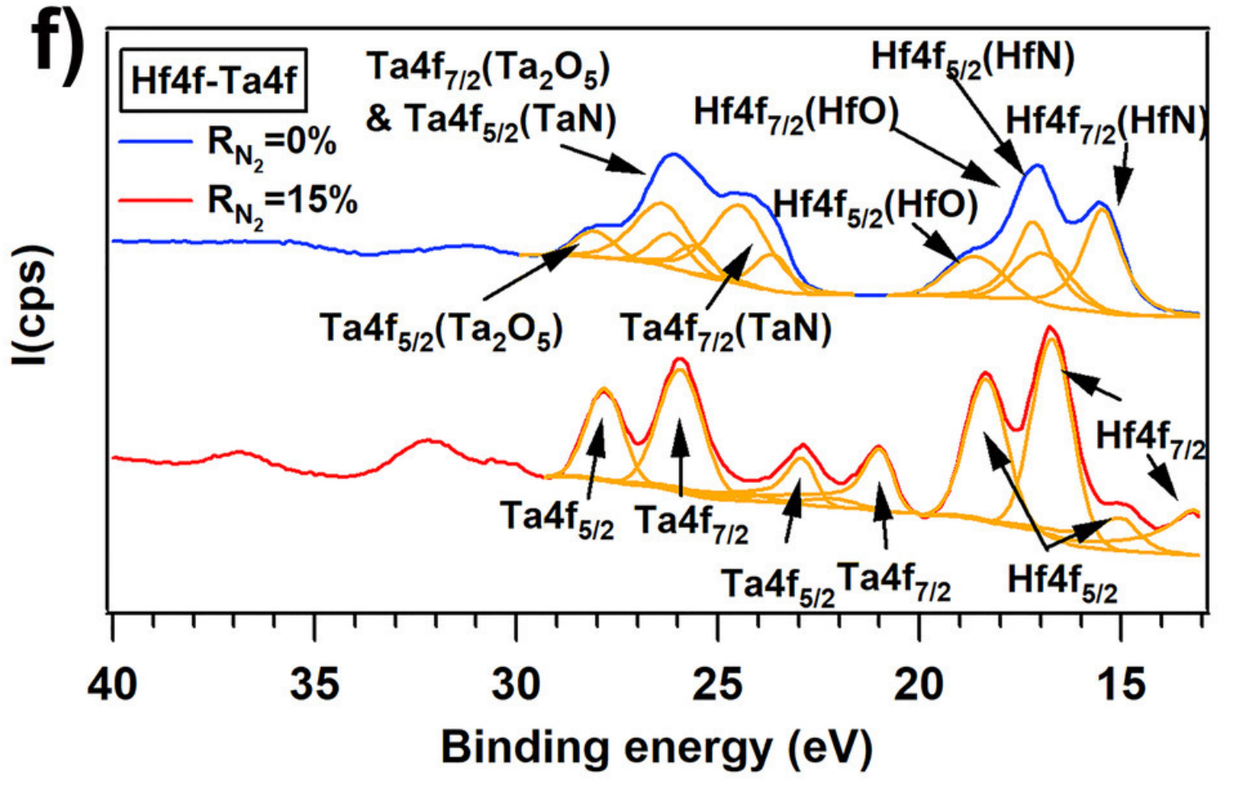
Hf4f-Ta4f
R_{N_2}=0%
R_{N_2}=15%
$Ta4f_{7/2}(Ta_2O_5)$ & $Ta4f_{5/2}(TaN)$
$Hf4f_{7/2}(HfO)$
$Hf4f_{5/2}(HfN)$
$Hf4f_{7/2}(HfN)$
$Hf4f_{5/2}(HfO)$
$Ta4f_{5/2}(Ta_2O_5)$
$Ta4f_{7/2}(TaN)$
$Ta4f_{5/2}$
$Ta4f_{7/2}$
$Ta4f_{5/2}$
$Ta4f_{7/2}$
$Hf4f_{5/2}$
$Hf4f_{7/2}$
I(cps)
40
35
30
25
20
15
Binding energy (eV)

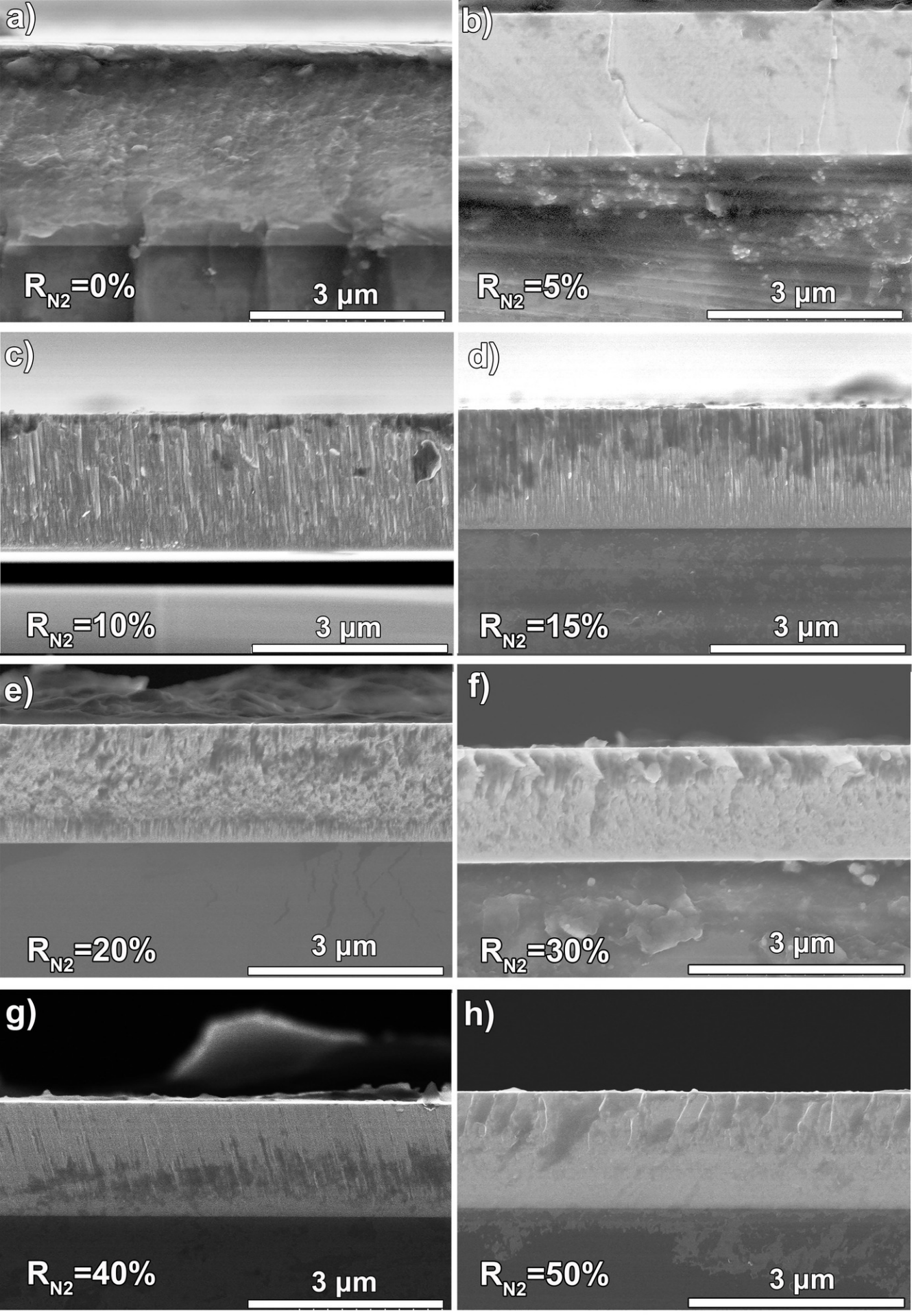
a)
R_{N2}=0%
3 μm
b)
R_{N2}=5%
3 μm
c)
R_{N2}=10%
3 μm
d)
R_{N2}=15%
3 μm
e)
R_{N2}=20%
3 μm
f)
R_{N2}=30%
3 μm
g)
R_{N2}=40%
3 μm
h)
R_{N2}=50%
3 μm

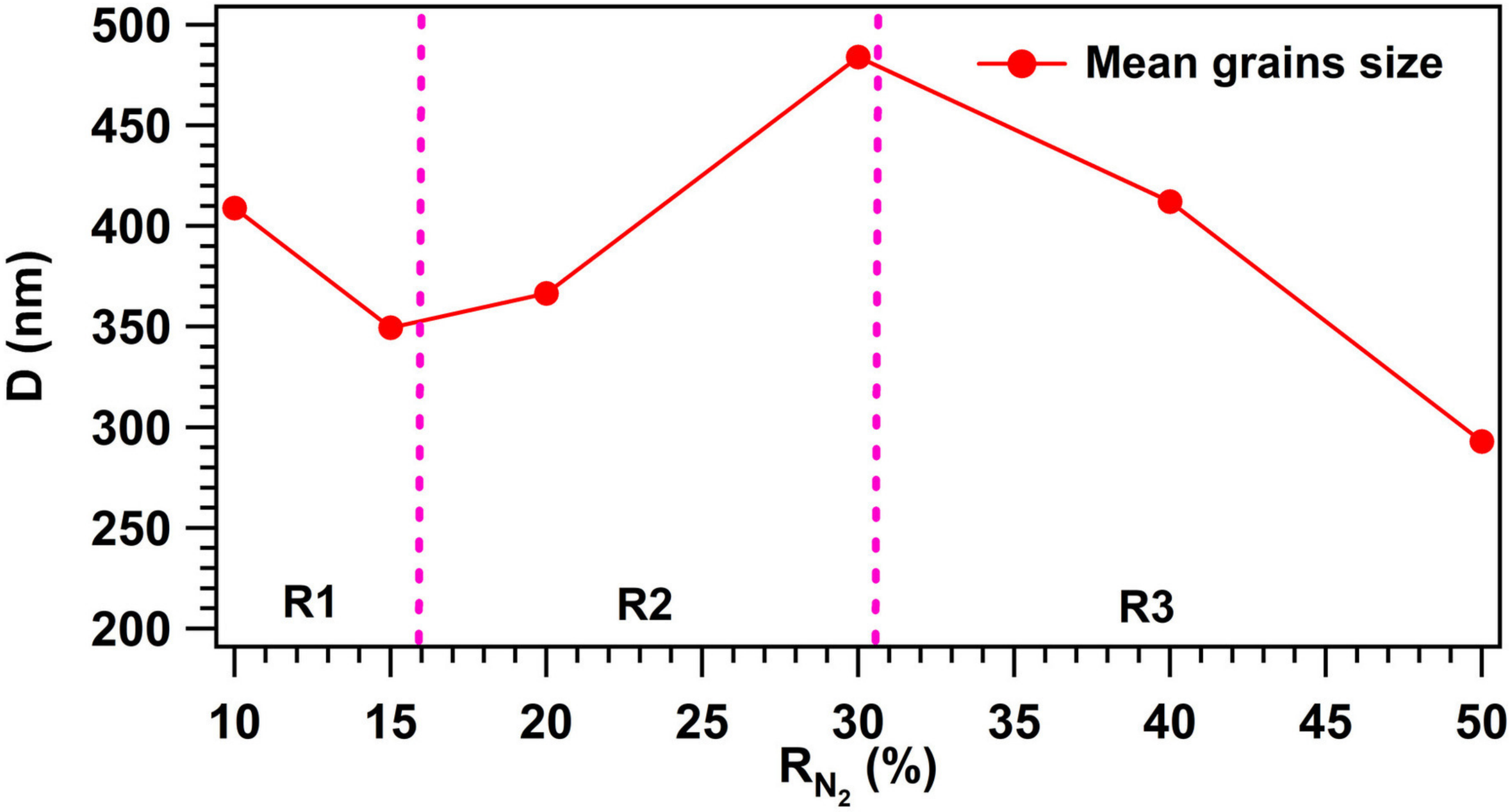
Mean grains size
D (nm)
500
450
400
350
300
250
200
R1
R2
R3
10
15
20
25
30
35
40
45
50
R_{N_2} (%)

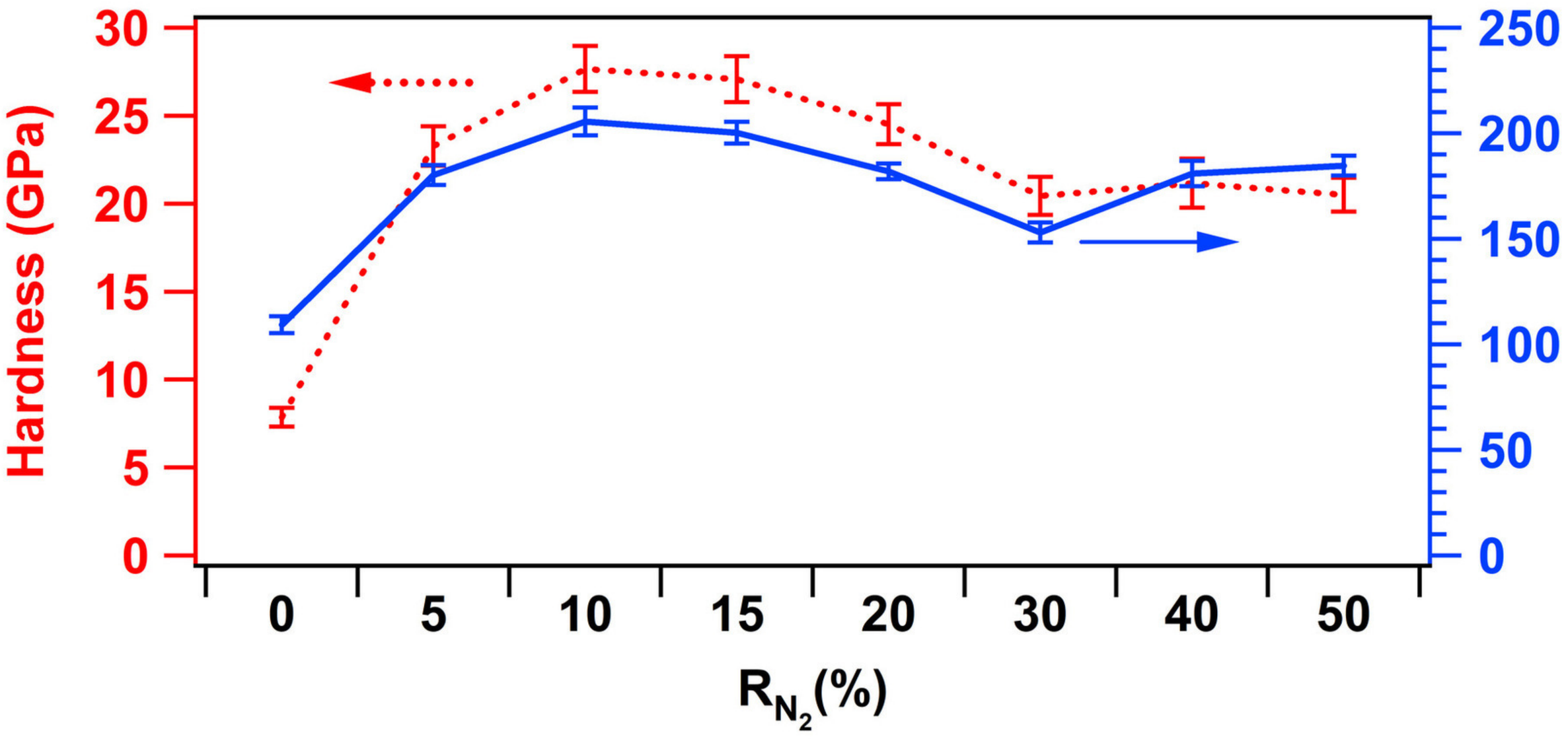
Hardness (GPa)
30
25
20
15
10
5
0
Young modulus (GPa)
250
200
150
100
50
0
0
5
10
15
20
30
40
50
R_{N_2}(%)

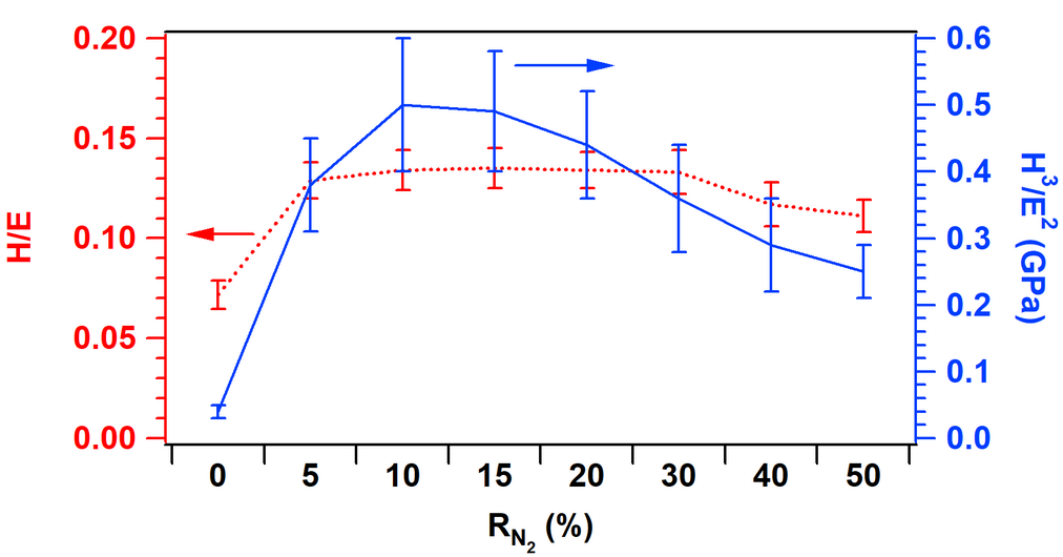
0.20
0.15
0.10
0.05
0.00
H/E
0.6
0.5
0.4
0.3
0.2
0.1
0.0
H3/E2 (GPa)
0
5
10
15
20
30
40
50
RN2 (%)

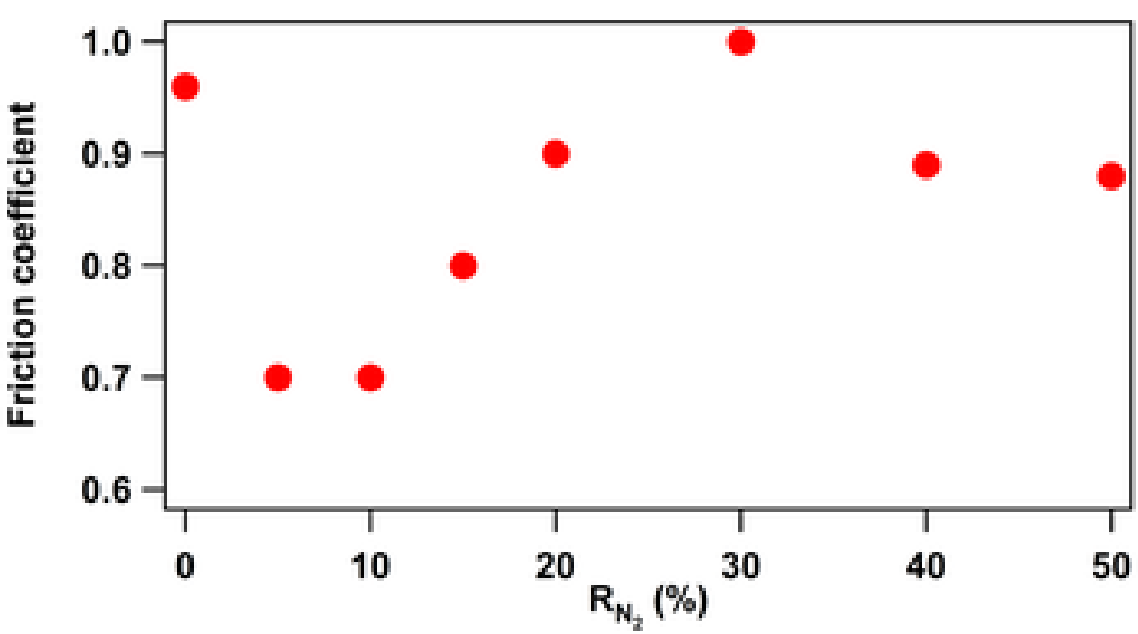
Friction coefficient
1.0
0.9
0.8
0.7
0.6
0
10
20
30
40
50
R_{N_2} (%)

Oxides		Nitrides	
Compounds	$\Delta Hf°$ ($KJ.mol^{-1}$)	Compounds	$\Delta Hf°$ ($KJ.mol^{-1}$)
Al_2O_3	-1675.69	AlN	-317.98
TiO_2	-891.2	TiN	-309.2
ZrO_2	-1042	ZrN	-336.8
Ta_2O_3	-1920	TaN	-230.2
HfO_2	-1145.5	HfN	-374.2